View metadata, citation and similar papers at core.ac.uk

brought to you by CORE

provided by epublications@Marquette

Marquette University
e-Publications@Marquette

Electrical and Computer Engineering Faculty Research and Publications

Electrical and Computer Engineering, Department of

9-23-2004

Micro-Switches with Sputtered Au, AuPd, Au-on-AuPt, and AuPtCu Alloy Electric Contacts

Ronald A. Coutu Jr.
Marquette University, ronald.coutu@marquette.edu

P. E. Kladitis
Air Force Institute of Technology

R. Cortez
Air Force Research Laboratory

R. E. Strawser
Air Force Research Laboratory

Robert L. Crane
Air Force Research Laboratory

Published version. *Proceedings of the 50th IEEE Holm Conference on Electrical Contacts and the 22nd International Conference on Electrical Contacts Electrical Contacts, 2004.* (September 23, 2004). DOI.
This material is declared a work of the U.S. Government and is not subject to copyright protection in the United States. Approved for public release; distribution is unlimited.
Ronald A. Coutu was affiliated with the Air Force Institute of Technology at the time of publication.

Micro-Switches with Sputtered Au, AuPd, Au-on-AuPt, and AuPtCu Alloy Electric Contacts

R.A. Coutu Jr.*, P.E. Kladitis*, R. Cortez†, R.E. Strawser†, and R.L. Crane‡
*Department of Electrical and Computer Engineering, Air Force Institute of Technology, Wright Patterson AFB, Ohio, 45433
Email: ronald.coutu@afit.edu or ronald.coutu@wpafb.af.mil
†Sensors Directorate - Air Force Research Laboratory, Wright Patterson AFB, Ohio, 45433
‡Materials and Manufacturing Directorate - Air Force Research Laboratory, Wright Patterson AFB, Ohio, 45433

Abstract— **This paper is the first to report on a new analytic model for predicting micro-contact resistance and the design, fabrication, and testing of microelectromechanical systems (MEMS) metal contact switches with sputtered bi-metallic (i.e. gold (Au)-on-Au-platinum (Pt), (Au-on-Au-(6%)Pt)), binary alloy (i.e. Au-palladium (Pd), (Au-(2%)Pd)), and tertiary alloy (i.e. Au-Pt-copper (Cu), (Au-(5%)Pt-(0.5%)Cu)) electric contacts. The micro-switches with bi-metallic and binary alloy contacts resulted in contact resistance between $1-2\ \Omega$ and, when compared to micro-switches with sputtered Au electric contacts, exhibited a 3.3 and 2.6 times increase in switching lifetime, respectively. The tertiary alloy exhibited a 6.5 times increase in switch lifetime with contact resistance ranging from 0.2–1.8 Ω.**

I. Introduction

Microelectromechanical systems (MEMS) switches are paramount in importance for the future miniaturization of radio frequency (RF) systems[1]. Space-based radar, phased array radar, and phase shifters all depend on reliably switching between RF loads. Because of their small geometries, exceptional RF performance, and low power consumption, MEMS contact switches, like that shown in Fig. 1, are ideally suited for these applications [1].

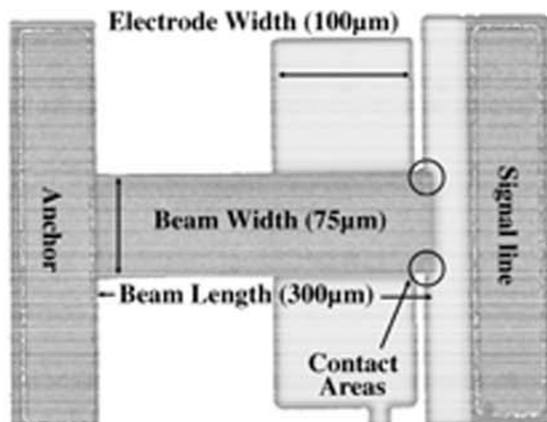

Fig. 1. A captured video image of a cantilever-style micro-switch.

[1]The views expressed in this article are those of the authors and do not reflect the official policy or position of the United States Air Force, Department of Defense, or the U.S. Government.

Important performance criteria for micro-switch applications are low contact resistance ($< 1-2\ \Omega$) and reliability ($> 10^8$ "hot-switched" switch cycles). The two primary failure mechanisms for MEMS metal contact switches are becoming stuck closed (i.e. stiction) and increased contact resistance with increasing switch cycles. Typically, micro-switches use gold-on-gold contacts to achieve low contact resistance. Gold (Au) is used due to its low resistivity and low susceptibility to oxidation and contaminant gettering. However, MEMS switches with Au contacts are prone to stiction and wear due to Au's relative low hardness (i.e. $\sim 1-2\ GPa$). The purpose of this work is to develop an analytic model for predicting micro-contact resistance and to fabricate micro-switches optimized for increased wear with low contact resistance.

When modeling micro-contact resistance, neglecting ballistic electron transport [2] and contaminant film resistance [3] underestimates contact resistance for low contact force applications. Majumder, et al. considered ballistic and diffusive electron transport by using Wexler's interpolation [4] and considered contact material deformation by using Hertz's elastic [5] and Chang, et al.'s elastic-plastic [6] (i.e. the CEB model) models [3]. Kogut and Komvopoulos derived an electrical contact resistance (ECR) model for conductive rough surfaces based on fractal geometry for the surface topography description, elastic-plastic deformation of contacting asperities, and size-dependent electrical constriction resistance of micro-contacts comprising the real contact area [7]. Additional work by Kogut and Komvopoulos resulted in an ECR model for conductive rough surfaces coated with a thin insulating layer based fractal geometry to describe the surface topography, elastic, elastic-plastic, and fully plastic deformation of surface asperities, and quantum mechanics considerations for the electric-tunnel effect through a thin insulating layer [8].

Majumder, et. al.'s model does not account for a contact load discontinuity in the CEB model and uses a Gamma function, needed for Wexler's interpolation, that is not well defined ($\Gamma(K=\infty) \neq 0$). Majumder, et al.'s Gamma function predicts ballistic and diffusive electron transport when the Knudsen number (K) goes to infinity which should be the completely ballistic region. In addition, the Kogut and Komvopoulos ECR models, as well as Majumder, et al.'s model, are based on the assumption that surface asperities have sufficient separation

US Government work not protected by US Copyright

and are independent.

In this work, the independent surface asperity assumption is no longer valid because sputtered electric contact films are used. A new micro-contact resistance model is developed using Chang's [9] improvements to the CEB model [6] and Mikrajuddin, et al.'s [10] derived Gamma function in Wexler's interpolation [4]. Lastly, contaminant film resistance is briefly investigated using measured contact resistance data.

In addition, previous micro-switch work focused on optimizing mechanical switch designs rather than investigating new contact metals [11]. Notable exceptions are Majumder, et al.'s and Duffy, et al.'s utilization of a "platinum group" and Pt contact metals, respectively [12], [13]. These metals were chosen over Au for their increased hardness and improved wear characteristics. In order to achieve acceptable contact resistance, Majumder, et al.'s micro-switches required multiple (i.e. 4 to 8), parallel contacts and were packaged in a hermetic environment while Duffy, et al.'s MEMS switches required actuation voltages approximately 45 V higher than the pull-in voltage. Schimkat studied Au-nickel (Ni) alloy (Au-(5%)Ni) macro-switch contacts in a low-force test configuration [14]. In this work, MEMS cantilever-style switches were designed and fabricated with sputtered bi-metallic (i.e. Au-on-Au-platinum (Pt), (Au-on-Au-(6%)Pt)), binary alloy (i.e. Au-palladium (Pd), (Au-(2%)Pd)), and tertiary alloy (i.e. Au-Pt-copper (Cu), (Au-(5%)Pt-(0.5%)Cu)) contact metals and hemispherical-shaped upper and planar lower contact geometries.

Generally, micro-switches with Au electric contacts are limited to approximately 10^6 "hot-switched" cycles because evaporated Au is a soft metal and prone to wear [12], [15]. Zavracky, et al. report $5{\cdot}10^8$ "hot-switched" cycles and over $2{\cdot}10^9$ "cold-switched" cycles for micro-switches that were packaged in nitrogen and had sputtered Au contacts [15]. Majumder, et al. reports greater than 10^7 "hot-switched" cycles and approximately 10^{11} "cold-switched" cycles for micro-switches with a "platinum group" contact metal [12]. In this work, test results for micro-switches with bi-metallic, binary alloy, and tertiary alloy contact metals are presented.

II. Contact Resistance Modeling

An understanding of contact mechanics is needed to design micro-sized electric contacts and predict contact resistance. There are two primary considerations; 1) how the contact material deforms (elastic, plastic, or elastic-plastic) and 2) the radius of the contact area.

A. Material Deformation Models

1) Elastic: When two surfaces intially come together, with low contact force, surface asperities (i.e. a-spots) undergo elastic deformation. Equations 1 and 2 define contact area and force for a single a-spot as a function of vertical deformation [9].

$$A = \pi R \alpha \tag{1}$$

where A is contact area, R is asperity peak radius of curvature, and α is asperity vertical deformation.

$$F_c = \frac{4}{3} E' \alpha \sqrt{R\alpha} \tag{2}$$

where F_c is the normal contact force and E' is the Hertzian modulus derived from

$$\frac{1}{E'} = \frac{1-\nu_1^2}{E_1} + \frac{1-\nu_2^2}{E_2} \tag{3}$$

where E_1 is the elastic modulus for contact one, ν_1 is Poisson's ratio for contact one, E_2 is the elastic modulus for contact two, and ν_2 is Poisson's ratio for contact two.

For circular areas (i.e. $A = \pi r^2$), (1) and (2) are related to the contact area radius (r) through Hertz's model [5]:

$$r = \sqrt[3]{\frac{3F_c R}{4E'}}. \tag{4}$$

When deformation is no longer reversible and the applied load is approximately three times the yield point (Y), ideal plastic material deformation begins [5].

2) Plastic: Plastic material deformation is modeled using Abbott and Firestone's well-known fully plastic contact model [16]. This model assumes that contact pressure is sufficiently large and has been applied long enough for all material creep to cease. Single asperity contact area and force are defined using (5) and (6):

$$A = 2\pi R \alpha \tag{5}$$

$$F_c = HA \tag{6}$$

where H is the Meyer hardness of the softer material [9].

Using (6), circular contact area radius is related to contact force through (7) [5]:

$$r = \sqrt{\frac{F_c}{H\pi}}. \tag{7}$$

An area discontinuity at the transition from ideal elastic to ideal plastic behavior is revealed when the elastic model from section II-A and this plastic model are used together [5]. The CEB model, discussed next, addresses this issue by assuming volume conservation of deformed surface asperities [6].

3) Elastic-Plastic: Elastic-plastic material deformation refers to when parts of the contact area are plastically deforming but encased by elastically deformed material. The CEB model describes material deformation that occurs between the ideal elastic and ideal plastic regions [17].

Equations 8 and 11 are the CEB model's contact area and force equations, respectively [6].

$$A = \pi R \alpha (2 - \frac{\alpha_c}{\alpha}) \tag{8}$$

where α_c is critical vertical deformation, where elastic-plastic behavior begins, given as:

$$\alpha_c = R(\frac{K_H H \pi}{2E'})^2. \tag{9}$$

US Government work not protected by US Copyright

where K_H is the hardness coefficient (assumed to be equal to 0.6 at the initial onset of plasticity [6]) given as:

$$K_H = 0.454 + 0.41\nu \quad (10)$$

where ν is Poisson's ratio.

$$F_c = K_H H A \quad (11)$$

In the CEB elastic-plastic model, a contact load discontinuity exists at the transition from elastic to elastic-plastic material deformation. Kogut and Etison addressed this by using finite element methods to model the elastic-plastic region with normalized contact force and area equations based on Hertzian elastic contact mechanics equations [18]. Chang observed that ideal plastic behavior normally occurred at $3Y$, not $K_Y Y$, where K_Y is the yield coefficient, and updated the CEB model using a linear interpolation [9]. Chang's new force equation for elastic-plastic material deformation is given by (12):

$$F_c = [3 + (\frac{2}{3}K_Y - 3)\frac{\alpha_c}{\alpha}]YA. \quad (12)$$

where $K_Y = 1.1282 + 1.158\nu$ [9].

The yield strength for most metals is related to its hardness through (13) [9]:

$$Y = 0.354H. \quad (13)$$

When K_Y and (13) are substituted into (12), Equation 14 results:

$$F_c = [1.062 + 0.354(\frac{2}{3}K_Y - 3(\frac{\alpha_c}{\alpha}))]HA. \quad (14)$$

Equations 8 and 14 represent the new CEB model [6] updated with Chang's improvements [9].

For circular areas, (14) is used to relate the contact area radius and the contact force through:

$$r = \sqrt{\frac{F_c}{H\pi[1.062 + 0.354(\frac{2}{3}K_Y - 3(\frac{\alpha_c}{\alpha}))]}}. \quad (15)$$

The contact area radius, determined from material deformation models, is a function of the contact force generated by the micro-switch.

B. Contact Force and Area

Contact force is a compressive force that causes material deformation by bulging [17]. Generally, MEMS switches are electrostatic devices that produce low contact forces ranging from tens of μN's up to a few mN's.

In micro-switches, contact force is defined by the mechanical switch design while contact area is defined by contact geometry, surface roughness, elastic modulus, and material hardness. From this description two contact area models have developed: 1) the multiple a-spot and 2) the single effective a-spot.

The multiple asperity model is based on Greenwood and Williamson's "asperity-based model" for elastic material deformation and Abbott and Firestone's "profilometric model" for plastic deformation [16], [19].

The assumptions used by Greenwood and Williamson follow: 1) rough contact surfaces are isotropic, 2) all surface asperity peaks are spherical with the same radii of curvature, 3) asperity height is randomly distributed, 4) asperities are far apart and independent, 5) material deformation occurs only in the asperities, and 6) no heating occurs. McCool studied anisotropic rough surfaces with randomly distributed elliptically asperities which revealed exceptional agreement with Greenwood and Williamson's simpler model [20]. Greenwood and Tripp showed that two rough contacting surfaces could be modeled by an equivalent single rough surface contacting a flat, smooth surface [21].

In the single effective asperity model, the individual contact spots are close together and their interactions are not independent. In this situation, the effective contact area is defined as the sum, not the parallel combination, of the individual contact areas. Fig. 2 illustrates the multiple a-spot and single effective a-spot models and the notion of an effective contact area radius (r_{eff}).

Majumder, et al. predicted a lower contact resistance bound when using the multi-asperity model and an upper contact resistance bound when using the single effective a-spot model [3].

The contact area radius dictates how electrons are transported through electrical connections. A brief discussion about the resistance resulting from ballistic, quasi-ballistic, and diffusive electron transport follows.

C. Contact Resistance and Electron Transport

Contact resistance (R_{C}), defined by (16), results from making electrical connections and considers the effects of constriction (R_{c}) and contaminant film (R_{cf}) resistances [5]:

$$R_{\text{C}} = R_{\text{c}} + R_{\text{cf}}. \quad (16)$$

Constriction resistance arises because electrical current can only flow through a-spots created during switch closure. "Classic" constriction resistance, based on diffusive electron

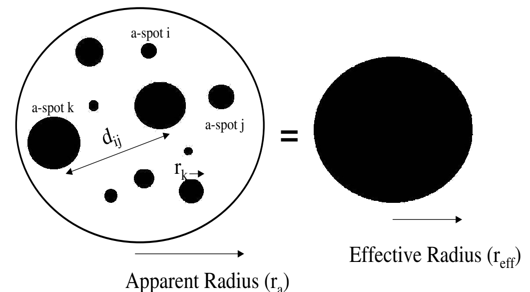

Fig. 2. Top view of the multiple asperity (left) and single effective asperity (right) contact area models.

US Government work not protected by US Copyright

transport, is modeled analytically using (17) which is based on Maxwellian spreading resistance theory [5]:

$$R_{\mathrm{c}} = \frac{\rho}{2r_{\mathrm{eff}}} \tag{17}$$

where R_{c} is constriction resistance and ρ is resistivity [5]. Constriction resistance is equal to contact resistance when contaminant film resistance is neglected.

When considering circular contact areas, (18) and (19) are the resulting "classic" macro-switch contact resistance equations that show $R_{\mathrm{c}} \propto F_{\mathrm{c}}^{(-\frac{1}{3})}$ for elastic deformation and $R_{\mathrm{c}} \propto F_{\mathrm{c}}^{(-\frac{1}{2})}$ for plastic deformation [5].

$$R_{\mathrm{cDE}} = \frac{\rho}{2}\sqrt[3]{\frac{4E'}{3F_{\mathrm{c}}R}} \tag{18}$$

where R_{cDE} is contact resistance for diffusive electron transport and elastic material deformation and

$$R_{\mathrm{cDP}} = \frac{\rho}{2}\sqrt{\frac{H\pi}{F_{\mathrm{c}}}} \tag{19}$$

where R_{cDP} is contact resistance for diffusive electron transport and plastic material deformation.

Micro-switches produce lower contact force than macro-switches which leads to smaller contact areas. When contact area radius is compared to an electron's elastic mean free path (l_{e}), the following electron regions are defined: ballistic, quasi-ballistic, and diffusive [22]. The ballistic region is when the elastic mean free path is greater than the effective contact radius (i.e. $l_{\mathrm{e}} > r_{\mathrm{eff}}$), the quasi-ballistic region is when $l_{\mathrm{e}} \sim r_{\mathrm{eff}}$, and the diffusive region is when $l_{\mathrm{e}} \ll r_{\mathrm{eff}}$ [3], [22]. The mean free path for most metals is approximately 500 $\mathring{A}$ [22]. Fig. 3 illustrates the ballistic and diffusive electron transport regions [22].

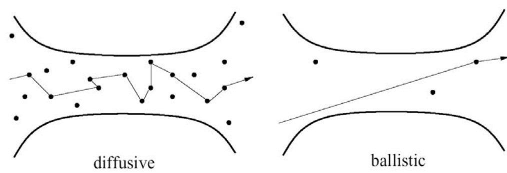

Fig. 3. Schematic illustration of diffusive (left) and ballistic (right) electron transport in a conductor [22].

Equation 20 or the Sharvin resistance is a semiclassical approximation for resistance when electrons exhibit ballistic transport behavior [22].

$$R_{\mathrm{S}} = \frac{4\rho K}{3\pi r_{\mathrm{eff}}} \tag{20}$$

where R_{S} is the so-called Sharvin resistance and K is the Knudsen number given as:

$$K = \frac{l_{\mathrm{e}}}{r_{\mathrm{eff}}}. \tag{21}$$

Wexler derived (22) as an interpolation between the ballistic and diffusive electron transport regions [4]:

$$\begin{aligned} R_{\mathrm{W}} &= \frac{4\rho K}{3\pi r_{\mathrm{eff}}}[1 + \frac{3\pi}{8}\Gamma(K)\frac{r_{\mathrm{eff}}}{l_{\mathrm{e}}}] \\ &= R_{\mathrm{S}} + \Gamma(K)R_{\mathrm{c}} \end{aligned} \tag{22}$$

where R_{W} is the so-called Wexler resistance and $\Gamma(K)$ is a slowly varying Gamma function of unity order [4].

Mikrajuddin, et al. derived a well behaved Gamma function from first principles:

$$\Gamma(K) \approx \frac{2}{\pi}\int_0^{\infty} e^{-Kx} Sinc(x)\,\mathrm{d}x \tag{23}$$

where Sinc(x) is defined as being equal to one when $x = 0$ and equal to $\frac{Sin(x)}{x}$ when $x \neq 0$ [10]. Fig. 4 is a plot of Mikrajuddin, et al.'s Gamma function that was solved using a recursive Newton-Cotes numerical integration formula.

D. New Micro-Contact Resistance Model

A new analytic micro-contact resistance model, based on the the single effective a-spot contact area model, is developed using Hertz's elastic [5], Chang's [9] improvements to the CEB model, Mikrajuddin, et al.'s [10] derived Gamma function, and Wexler's interpolation from ballistic to diffusive electron transport [4]. The single effective a-spot contact area model is needed because the independence of the surface asperities can no longer be assumed when using sputtered contact films with low surface roughness (i.e. $\approx 30 - 50$ $\mathring{A}$) and tightly packed material grain structures (i.e. ≈ 50 $\mathring{A}$ in diameter). In addition, the micro-switch's contact geometries (i.e. hemispherical-shaped upper and planar lower) match the elastic and elastic-plastic material deformation models presented earlier.

For circular contact areas and elastic material deformation, a contact resistance equation is derived for the ballistic electron transport region by substituting (4) into (20) resulting in:

$$R_{\mathrm{cBE}} = \frac{4\rho K}{3\pi}\sqrt[3]{\frac{4E'}{3F_{\mathrm{c}}R}} \tag{24}$$

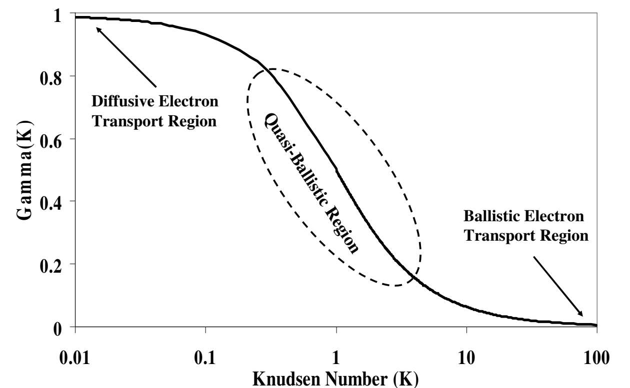

Fig. 4. A plot of Mikrajuddin, et al.'s derived Gamma function.

US Government work not protected by US Copyright

where $R_{\rm cBE}$ is the contact resistance for ballistic electron transport and elastic deformation.

Equation 25, the new micro-contact resistance model for elastic deformation, results when (24) and (18) are substituted into (22):

$$R_{\rm WE} = R_{\rm cBE} + \Gamma(K) R_{\rm cDE} \tag{25}$$

where $R_{\rm WE}$ is the Wexler resistance for elastic material deformation.

Equation 26 is a contact resistance equation based on ballistic electron transport and elastic-plastic material deformation and is found by substituting (15) into (20).

$$R_{\rm cBEP} = \frac{4\rho K}{3\pi}\sqrt{\frac{H\pi[1.062 + 0.354(\frac{2}{3}K_{\rm Y} - 3(\frac{\alpha_{\rm c}}{\alpha}))]}{F_{\rm c}}} \tag{26}$$

Equation 27 is a contact resistance equation based on diffusive electron transport and elastic-plastic material deformation and is found by substituting (15) into (17).

$$R_{\rm cDEP} = \frac{\rho}{2}\sqrt{\frac{H\pi[1.062 + 0.354(\frac{2}{3}K_{\rm Y} - 3(\frac{\alpha_{\rm c}}{\alpha}))]}{F_{\rm c}}} \tag{27}$$

Equation 28, the new micro-contact resistance model for elastic-plastic deformation, results when (26) and (27) are substituted into (22):

$$R_{\rm WEP} = R_{\rm cBEP} + \Gamma(K) R_{\rm cDEP} \tag{28}$$

where $R_{\rm WEP}$ is the Wexler resistance for elastic-plastic material deformation.

III. MEMS SWITCHES

A brief discussion of the design, fabrication, and testing of the micro-switches in this study, shown in Fig. 1, is presented next.

A. Design

In metal contact micro-switches, initial switch closure is defined by the pull-in voltage. At pull-in physical contact between the upper (i.e. dimples) and lower contacts is first established with minimal contact force. As the actuation voltage is increased, contact force also increases and material deformation causes the contact area to increase. After pull-in, the micro-switch is modeled as a deflected beam with a fixed end, a simply supported end, and an intermediately placed load as illustrated in Fig. 5.

Using a parallel plate capacitor model and neglecting fringing fields, the intermediately placed load is modeled as:

$$F_{\rm e} = \frac{\epsilon_{\rm o} A_{\rm sa} V^2}{2g^2} \tag{29}$$

where $F_{\rm e}$ is the electrostatic force, $\epsilon_{\rm o}$ is the permittivity of free space, $A_{\rm sa}$ is the surface area of the smaller parallel plate, V is the actuation voltage, and g is the gap between the plates [23].

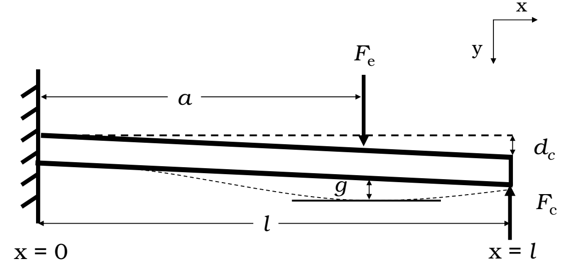

Fig. 5. Cantilever beam model with a fixed end at $x = 0$, a simply supported end at $x = l$, and an intermediately placed load ($F_{\rm e}$) at $x = a$.

Equation 30 is the resulting contact force equation:

$$F_{\rm c} = [\frac{F_{\rm e} a^2}{2l^3}(3l - a) - \frac{E I_{\rm z} d_{\rm c}}{l^3}] \tag{30}$$

where $F_{\rm c}$ is contact force, a is the location of the electrostatic force, l is beam length, $d_{\rm c}$ is beam tip deflection distance, and $I_{\rm z}$ is the area moment of inertia about the z-axis defined by:

$$I_{\rm z} = \frac{wt^3}{12} \tag{31}$$

where w is the beam width and t is the beam thickness [24].

Micro-switch contact force, illustrated by Fig. 6, is mapped to actuation voltage using (30).

After completing the micro-switch mechanical design, using (29) through (31), a compatible thin film deposition process (i.e. co-sputtering) was chosen and candidate electric contact metal alloys were selected.

B. Fabrication

The micro-switches in this study were fabricated on highly resistive sapphire substrates. Four wafers of devices, each with a different contact metallurgy (i.e. sputtered Au, Au-on-Au-(6%)Pt, Au-(2%)Pd, and Au-(5%)Pt-(0.5%)Cu) were individually fabricated using the process illustrated in Fig. 7. Refer to Fig. 7 for the following discussion.

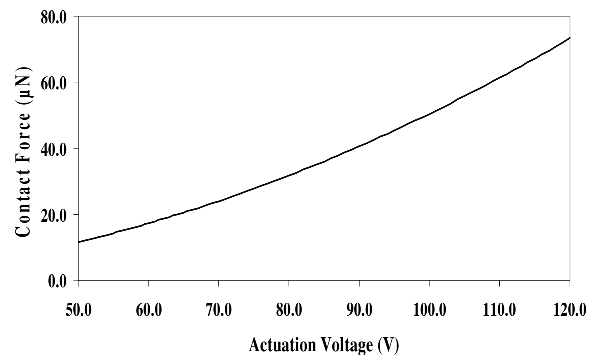

Fig. 6. Micro-switch contact force (per contact) plot.

US Government work not protected by US Copyright

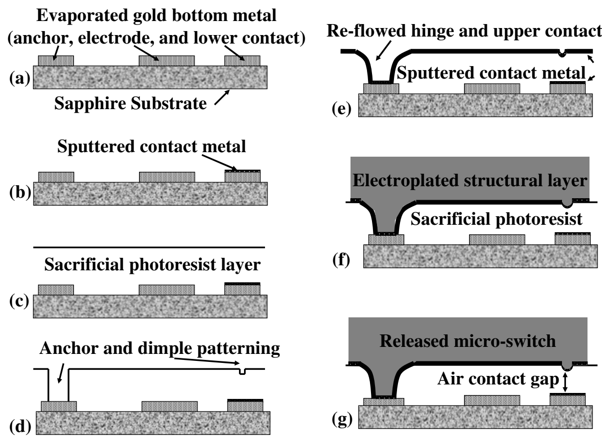

Fig. 7. Illustration of the micro-switch fabrication process.

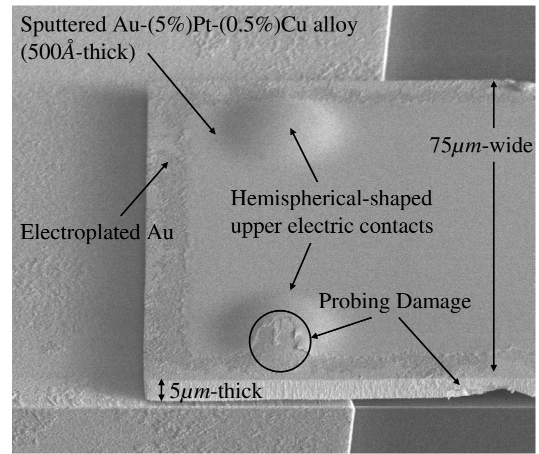

Fig. 8. Scanning electron micrograph (SEM) image showing the hemispherical-shaped upper contacts and the sputtered electric contact metal. Probing damage occurred while flipping the cantilever beam for imaging.

The actuation electrode and lower electric contact layers were approximately 3000 $\AA$ of evaporated Au patterned using a standard metal lift-off technique (**a**) [25]. A thin (200 $\AA$-thick) chromium (Cr) layer was used under the evaporated Au layer to help the Au remain adhered to the substrate. The lower electric contact metal was sputter deposited (500 $\AA$-thick) and patterned using a metal lift-off technique (**b**).

The beam's gap or sacrificial layer was approximately 3 μm-thick and created using MicroChem's polydimethylglutarimide (PMGI) based photoresist (**c**) [26]. The micro-switch's hinge geometry was defined in the sacrificial photoresist using standard photolithography techniques while the upper contact geometries were defined by a partial expose and develop of the sacrificial photoresist layer (**d**). A timed re-flow in an oven with flowing nitrogen was used to reform the dimple into a hemispherical-shaped upper contact bump (**e**).

The upper contact metals were also sputter deposited (500 $\AA$-thick), and patterned using standard photolithography techniques (**e**). The upper contact material, located on the underside of the cantilever beam, is highlighted in Fig. 8.

After electroplating the cantilever's gold structural layer (5 μm-thick) (**f**), the devices were released using a CO_2 critical point dryer and tested to ensure proper operation and performance (**g**).

C. Test Results

A series of five micro-switches were tested on four different wafers (20 switches total) to experimentally characterize contact resistance and micro-switch lifetime. The experimental setup is illustrated in Fig. 9.

The micro-switches were tested by wafer probing using an Alessi Rel-4100A microprobe station with standard microprobes. The actuation voltage was applied using an HP 3245A universal source and a Krohn-Hite wideband amplifier. Closed switch resistance was measured using an HP 3458A multimeter in a four-point probe configuration. Contact resistance was found by subtracting the measured beam resistance from the closed switch resistance measurements.

During contact resistance testing, a voltage ranging from 0 to 120 V in 0.5 V increments was applied between the cantilever beam and the actuation electrode. The micro-switch closes when the actuation voltage exceeds the pull-in voltage. As the applied voltage is increased, beyond the pull-in voltage, contact force increases and contact resistance decreases. Contact resistance data were collected each time the actuation voltage was incremented. This test was accomplished twice for each micro-switch with approximately 10-15 seconds between the experiments. The average minimum contact resistance data, with 120 V of applied actuation voltage, are summarized in Table I. For comparison, simulated contact resistance values, calculated using measured material properties and (28), are also provided in Table I.

Table I shows that the average minimum contact resistance is higher than the simulated values. This discrepancy is partly

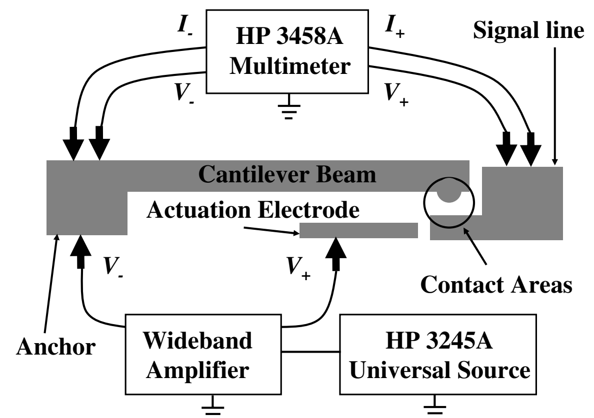

Fig. 9. Experimental test set up used to measure pull-in voltage, contact resistance, and switch lifetime.

US Government work not protected by US Copyright

TABLE I
AVERAGE MINIMUM CONTACT RESISTANCE (R_c) AND STANDARD DEVIATION FOR MEASURED DATA. SIMULATED R_c WAS FOUND USING MEASURED MATERIAL PROPERTIES AND (28).

Metal/Alloy	R_c / StdDev Experiment 1	R_c / StdDev Experiment 2	R_c Simulated
Au	0.94 / 0.20	0.83 / 0.19	0.096
Au-(2%)Pd	0.63 / 0.19	0.49 / 0.07	0.165
Au-on-Au-(6%)Pt	0.73 / 0.13	0.67 / 0.16	0.136
Au-(5%)Pt-(0.5%)Cu	0.34 / 0.33	0.33 / 0.30	0.197

due to adsorbed contaminant films on the electric contact's surface. This hypothesis is backed by contact resistance, collected during experiment two, that is lower than data collected for experiment one. It appears that a contaminant film has been "wiped" away during experiment one resulting in "cleaner" contacts for experiment two.

Contact resistance data, from a representative micro-switch with Au electric contacts, and simulated contact resistance, calculated using (25), (28), and measured material properties, are plotted on Fig. 10. The data on Fig. 10 shows a sharp decrease in contact resistance at approximately $\sim 93\ V$ for micro-switches tested the first time. This drop in measured contact resistance was consistent and occurred between 90 V and 98 V for all the micro-switches tested. We believe this anomaly was caused by the fritting of a contaminant film [27]. During experiment two this anomaly was less drastic, most likely, because the contaminant film was "cleaned" off the contact than during the first experiment.

Fig. 11 shows measured and simulated contact resistance for micro-switches with Au-(5%)Pt-(0.5%)Cu electric contacts. The measurements, shown on Fig. 11, are somewhat lower than the simulated values and fritting is less obvious. We believe this is a result of the single effective asperity model, used in this study, not accurately representing the actual contact area for these micro-switches. Recall that Majumder, et

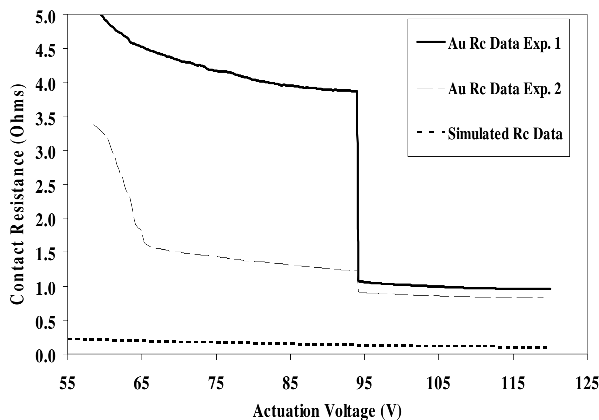

Fig. 10. Contact resistance (R_c) data for a representative micro-switch with sputtered Au electric contacts.

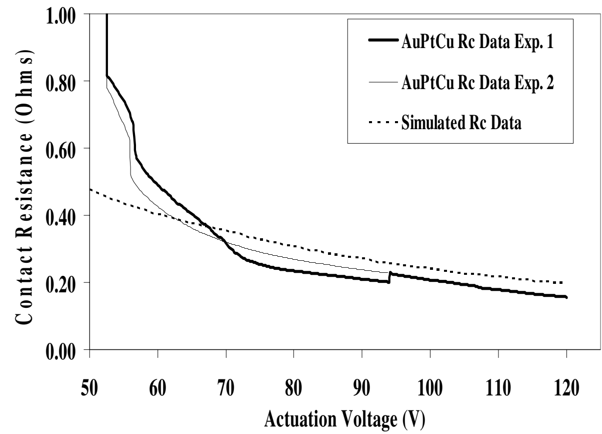

Fig. 11. Contact resistance (R_c) data for a selected micro-switch with Au-(5%)Pt-(0.5%)Cu electric contacts.

al. showed a contact resistance lower limit using the multiple asperity-based model and an upper limit using the single effective asperity-based mode. This may indicate that the Au-(5%)Pt-(0.5%)Cu films have larger material grains and higher surface roughness and are better represented using the multi-asperity contact area model.

In addition, during experiment one a resistance increase from 0.20 to 0.22 Ω was measured at $\sim 93\ V$. We believe that localized contact area heating caused the tertiary contact alloy to change phase or form an intermetallic compound resulting in this small increase in resistance. This hypothesis is backed by resistance data, collected during the second experiment, that are higher than data from the first experiment (i.e. between 70 V and 93 V). For actuation voltages higher than $\sim 93\ V$ the measured resistance values from both experiments agree. This may indicate that the contact material was in a stable phase during the second experiment. This anomaly was most likely not observed in the micro-switches with binary alloy contacts because their alloy compositions avoided miscibility gaps and the formation of intermetallic compounds [28].

During lifecycle testing, the micro-switches were actuated with a 50% duty cycle square wave input. The waveform's "on" voltage level was set to the pull-in voltage plus approximately 1-3 V for increased contact force. The input waveform's frequency was set below the beam's resonant frequency. The micro-switches were cycled continuously until they failed open (i.e. infinite resistance) or closed (i.e. stuck down). Contact resistance data were collected every 30 seconds by increasing the input waveform's duty cycle to 90% and lowering its frequency to 1 Hz for 2 seconds. The multimeter's open circuit voltage ($\sim 8.2\ V$) was present on the contacts for all the switching events (i.e. "hot-switching"). The success criteria for this testing was measured contact resistance less than $\sim 2\ \Omega$ and infinite open switch resistance.

Micro-switch contact resistance versus switch cycles is plotted on Fig. 12. The raw data was curve fitted with trendlines for selected micro-switches with different contact metals.

US Government work not protected by US Copyright

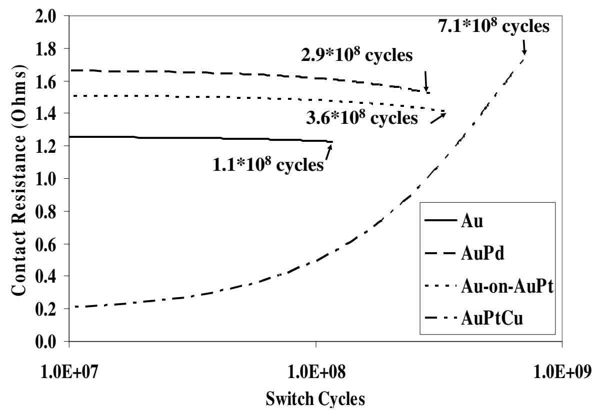

Fig. 12. Contact resistance versus switch cycles data plot.

The micro-switches with bi-metallic (Au-on-Au-(6%)Pt) and binary alloy (Au-(2%)Pd) contacts resulted in contact resistance between $1-2\ \Omega$ and, when compared to micro-switches with sputtered Au electric contacts, exhibited a 3.3 and 2.6 times increase in switching lifetime, respectively. The micro-switches with tertiary alloy (Au-(5%)Pt-(0.5%)Cu) contacts exhibited a 6.5 times increase in switch lifetime with contact resistance ranging from 0.2–1.8 Ω. This was most likely due to the increased material hardness of the sputtered metal alloys. Also, the micro-switches with sputtered Au contacts outperformed other micro-switches with Au contacts [12]. Once again, this was most likely due to the increased material hardness of the sputtered Au contact metals. The measured Meyer hardness of evaporated Au, sputtered Au, Au-(2%)Pd, Au-(6%)Pt, and Au-(5%)Pt-(0.5%)Cu thin films were approximately 1.0 GPa, 1.7 GPa, 1.9 GPa, 2.0 GPa, and 2.2 GPa, respectively.

The micro-switches with Au-(5%)Pt-(0.5%)Cu contacts exhibited increased contact resistance with increased numbers of switch cycles. The plot on Fig. 12 shows a steady rise in contact resistance between 10^7 and $7.1{\cdot}10^8$ switch cycles. This may indicate that a contaminant film, induced by contact wear, was developing. This hypothesis is supported by the high closed switch resistance failure mechanism observed while testing these micro-switches. The other micro-switches, with Au and binary alloy contacts, all failed due to stiction.

IV. Conclusions

The purpose of this work was to develop a new analytic contact resistance model for micro-switches employing hemispherical-shaped upper contacts and sputtered contact metals, and to show the design, fabrication, and test results for micro-switches with metal alloy electric contacts. Overall, the results show increased micro-switch wear performance at the expense of a small increase in contact resistance for devices with bi-metallic, binary alloy, and tertiary alloy contacts.

Acknowledgment

This work was sponsored by the Materials and Manufacturing Directorate, Air Force Research Laboratory, USAF, under project order number QGWSML02722002, POC: Dr. Robert L. Crane. The authors would like to acknowledge the Sensors Directorate, Air Force Research Laboratory, in particular, Dr. Rob Reid, Dr. LaVern Starman, Dr. Jack Ebel, and Dr. Kevin Leedy for design inputs and assistance with the fabrication process.

References

[1] G. Rebeiz, *RF MEMS Theory, Design, and Technology*, (New Jersey: John Wiley & Sons, Inc.), 2003.
[2] S. Bromley and B. Nelson, "Performance of Microcontacts Tested with a Novel MEMS Device," 47th *IEEE Holm Conference on Electrical Contacts*, pp 122–127, 2001.
[3] S. Majumder, et al., "Study of contacts in an electrostactically actuated microswitch," *Sens. and Act. A.*, **93:1**, pp 19–26, 2001.
[4] G. Wexler, "The size effect and the non-local Boltzmann transport equation in orifice and disk geometry," *Proc. Phys. Soc.*, **89**, pp 927–941, 1966.
[5] R. Holm, *Electric Contacts: Theory and Applications*, (Berlin: Springer), 1969.
[6] W. Chang, I. Etison, and D. Bogy, "An elastic-plastic model for the contact of rough surfaces" *ASME J. of Tribol.*, **109**, pp 257–263, 1987.
[7] L. Kogut and K. Komvopolous, "Electrical contact resistance theory for conductive rough surfaces" *Amer. Inst. of Phys.*, **94:5**, pp 3153–3162, 2003.
[8] L. Kogut and K. Komvopolous, "Electrical contact resistance theory for conductive rough surfaces separated by a thin insulating film," *Amer. Inst. of Phys.*, **95:2** pp 576–585, 2003.
[9] W. Chang, "An elastic-plastic model for a rough surface with an ion-plated soft metallic coating," *J. of Wear*, **212**, pp 229–237, 1997.
[10] A. Mikrajuddin, F. Shi, H. Kim, and K. Okuyama, "Size-dependent electrical constriction resistance for contacts of arbitrary size: from Sharvin to Holm limits," *Mat. Sci. in Semi. Proc.*, **2** pp 321–327, 1999.
[11] D. Peroulis, S. Pacheco, K. Sarabandi, and L. Katehi, "Electromechanical considerations in developing low-voltage RF MEMS switches," *IEEE Trans. on MTT*, **51:1**, pp 259–70, 2003.
[12] S. Majumder, J. Lampen, R. Morrison, and J. Maciel, "MEMS Switches," *IEEE Instr. and Meas. Mag.*, pp 12–15, 2001.
[13] S. Duffy, et al., "MEMS microswitches for reconfigurable microwave circuitry," *IEEE Micro. and Wire. Comp. Lett.*, **11:3**, pp 106–108, 2001.
[14] J. Schimkat, "Contact measurements providing basic design data for microrelay actuators," *Sens. and Act. A.*, **73**, pp 138–143, 1999.
[15] P. Zavracky, S. Majumder, and N. McGruer, "Micromechanical switches fabricated using nickel surface micromachining," *J. of MEMS*, **6:1**, pp 3–9, 1999.
[16] E. Abbot and F. Firestone, "Specifying surface quantity - a method based on the accurate measurement and comparison," *ASME Mech. Eng.*, **55**, pp 569, 1933.
[17] C. Calladine, *Plasticity for Engineers*, (Ellis Horwood Limited: Chichester), 1985.
[18] L. Kogut and I. Etsion, "Elastic-Plastic Contact Analysis of a Sphere and a Rigid Flat" *J. of Applied Mech.*, **69**, pp 657–662, 2002.
[19] J. Greenwood and J. Williamson, "Contact of nominally flat surfaces," *Proc. Royal Soc. A.* **295**, p 257–263, 1966.
[20] J. McCool, "Predicting microfracture in ceramics via a microcontact model," *ASME J. of Tribol.* **108**, pp 380–386, 1986.
[21] J. Greenwood and J. Tripp, "The contact of two nominally flat rough surfaces," *Proc. Inst. of Mech. Eng.*, **185**, pp 625–633, 1971.
[22] N. Agraït, "Quantum properties of atomic-sized conductors," *Physics Reports*, **377** pp 81–279, 2003.
[23] G. Kovacs, *Micromachined Transducers Sourcebook*, (New York: McGraw-Hill, Inc.), 1998.
[24] J. Shigley and C. Mischke, *Mechanical Engineering Design, Fifth Edition*, (New York: McGraw-Hill, Inc.), 1990.
[25] M. Madou, *Fundamentals of Microfabrication, Second Edition*, (Boca Raton: CRC Press), 2002.
[26] MicroChem Corp., http://www.microchem.com, 2003.
[27] D. Hyman and M. Mehregany, "Contact physics of gold microcontacts for MEMS microswitches" *IEEE Trans. on Comp. and Pack. Tech.* **22:3** pp 357–64, 1992.
[28] H. Okamato, Ed., *Binary Alloy Phase Diagrams, Second Edition*, (Ohio: ASM International), 1992.

US Government work not protected by US Copyright